PAPER • **OPEN ACCESS**

Remote measurement of cardiopulmonary signal using an unmanned aerial vehicle

To cite this article: Ali Al-Naji *et al* 2018 *IOP Conf. Ser.: Mater. Sci. Eng.* **405** 012001

IOP Conf. Series: Materials Science and Engineering **405** (2018) 012001 doi:10.1088/1757-899X/405/1/012001

Remote measurement of cardiopulmonary signal using an unmanned aerial vehicle

Ali Al-Naji[1,2]*, Asanka G. Perera[1] and Javaan Chahl[1, 3]

[1] School of Engineering, University of South Australia, Mawson Lakes, Australia
[2] Electrical Engineering Technical College, Middle Technical University, Iraq
[3] Joint and Operations Analysis Division, Defence Science and Technology Group, Melbourne, Australia

*ali_abdulelah_noori.al-naji@mymail.unisa.edu.au

Abstract. This study proposes a computer vision-based system to reveal the cardiopulmonary signal of humans in both static and dynamic scenarios without the need for restricting or contact. The proposed system extracts the signal based on the optical properties of skin colour variations in the facial region using image sequence analysis captured by a hovering drone while being convenient, safe and also cost-effective. The experimental results showed very good agreement, strong correlation coefficients and acceptable error ratios in comparison to reference instruments (finger pulse oximeter and Piezo respiratory belt). Therefore, the proposed system in this paper may be suitable to be applied to detect human physiological parameters in war zones and natural disasters when the contact with the subject is difficult or impossible.

1. Introduction

Measurement of physiological parameters is often essential to maintain individuals' health because of its primary role in the diagnosis of health conditions and monitoring of wellbeing. Current monitoring systems rely on direct contact and require a variety of sensors and electrodes to be attached to patients for long periods, in both clinical and home environments. These systems are restrictive, uncomfortable and potentially unsafe [1-6]. Therefore, there is a need to monitor physiological parameters when contact with skin is either undesirable or is not possible. With rapid growth of remote measurement technology, unobtrusive cardiopulmonary activity monitoring has become feasible.

Interesting research has been undertaken using many remote technologies to detect cardiopulmonary signal, including Doppler effect-based technologies [7-12], thermal imaging technologies [13-18] and imaging photoplethysmography (iPPG) technologies [19-24]. All these remote technologies rely on the observation of physiological and physical variations resulting from the cardiopulmonary activity such as skin colour variations, head motion, arterial pulse motion, thorax motion [25, 26]. However, Doppler and thermal imaging technologies generally need specialised hardware and are somewhat expensive [25, 27]. In addition, Doppler technologies may cause some biological effects on human tissue [13, 25, 27]. In contrast, the iPPG technologies seem to be the most promising methods for remote physiological assessments [25, 27]. But one of the most challenges facing iPPG technologies is when cardiopulmonary signal mix with noise and motion artefacts signal [28]. Many studies proposed different algorithms for noise artefacts removal from the iPPG signal. some examples, including principal component analysis (PCA) [29], independent component analysis (ICA) [22, 23], canonical correlation analysis (CCA.) [19,

30], ensemble empirical mode decomposition (EEMD) [20, 31, 32], chrominance (CHRO) [33], support vector regression (SVR) [21], spatial-subspace rotation (2SR) [34] and partial least squares (PLS) [35]. However, each algorithm has its strengths and weaknesses under different conditions, leading to some challenges and problems that have to be addressed [25].

In this study, a computer vision-based iPPG is proposed to extract the cardiopulmonary signal (heart rate HR and respiratory rate RR) from a hovering unmanned aerial vehicle (UAV) and remove the noise and motion artefacts using a new algorithm using signal decomposition technique based on complete ensemble EMD and ICA technique.

2. Materials and methods

2.1. Research ethics

The research ethics clearance was obtained from the Human Research Ethics Committee (HREC) at the University of South Australia (UniSA). Our research participants had consented to take part in this study and for the use of data that were captured from the UAV after a full explanation of the study procedures. For asset protection and privacy purposes, all collected video data were stored on a secure computer at the UniSA and will not be available for public use.

2.2. Participants and validation methods

This study was performed using 8 participants (4 males and 4 females) aged from 24 to 38 years. The video data were captured using a hovering UAV (3DR solo drone, 10MP, 5.4 mm GoPro Lens) with a resolution of 3840 × 2160 and a frame rate of 25 fps at a distance of 3 meters from the participant as shown in Figure 1. All participants were asked to breathe normally while doing some static and dynamic scenarios (normal talking, blinking, head rotation and facial expression). The validation procedure was carried out considering the measured data provided by a Rossmax SA210 pulse oximeter and MLT1132 Piezo respiratory belt transducer.

Figure 1. Data collection using the UAV (3DR solo drone)

2.3. System framework

Several image and signal processing techniques were considered in the design of the proposed system in this study to extract the relevant features from the facial video signal and eliminate noise artefacts embedded in the image spatial domain. These techniques include skin colour magnification technique, signal decomposition technique, ICA technique, spectral analysis method, band-pass filters and peak detection. The system framework of the proposed system is presented in Figure 2.

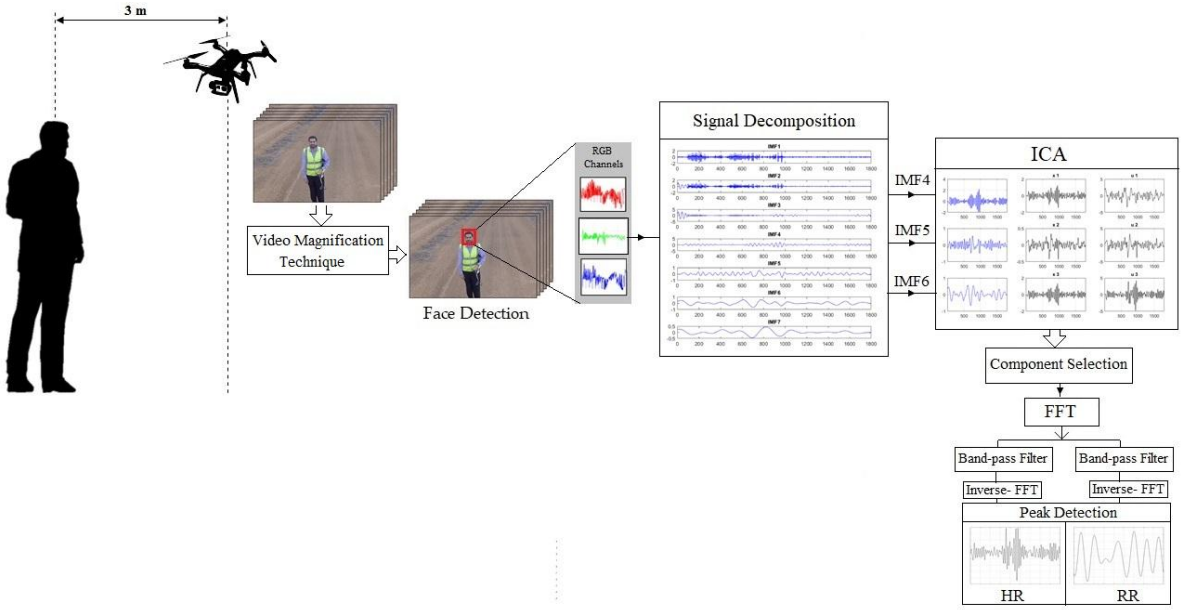

Figure 2. The system framework of the proposed system

2.3.1. Skin colour magnification

The skin colour variations in the participant's face are volumetric changes in the blood caused by the pressure changes during cardiac cycle. The colour of blood varies due to the exchange of gases through the cardiopulmonary activity, which also affects the skin colour. These variations in the skin colour are difficult to recognise. Therefore, a standard video magnification technique [36] was used to magnify these variations. The green (G) component was only selected and magnified 20x with band-pass filtering of 0.15 Hz to 3 Hz since this component contains the most harmonic cardiac signal among the other components (i.e. red and blue) [19, 22, 23, 37].

2.3.2. Face detection

To enhance results accuracy and efficiency, a face detection algorithm proposed by Liao et al. [38], was used in this study to select the facial region of interest (ROI). This face detection algorithm is a robust method to the challenges associated with unconstrained faces (e.g. inclined or angled faces, face rotation and faces in a crowd). The locations of the eyes and mouth for the selected ROI were also removed to reduce the noise artefacts generating from blinking and talking during videoing. The time-series signal, $x\,(t)$, was calculated by averaging of all the image pixel intensities in the selected ROI as follows:

$$x\,(t) = \frac{\sum_{a,b \in ROI} I\,(a,b,t)}{|ROI|} \tag{1}$$

where $I(a,b,t)$ is the pixel intensity at location (a,b) and time (t), and $|ROI|$ is the size of the selected region.

2.3.3. Signal decomposition

Signal decomposition is a powerful representation scheme for multiscale signal and image analysis that is used to get information from the nonstationary time-varying signals. Empirical mode decomposition (EMD) [39] is one of the most commonly used decomposition techniques to reduce the noise artefacts from biomedical signals [40-42]. This technique decomposes a non-linear and/or non-stationary signal into a set of components, namely intrinsic mode functions (IMFs), and selecting the most informative components to represent the original signal. Later on, a noise-assisted signal decomposition technique,

called ensemble EMD (EEMD), was proposed by Wu and Huang [43] to solve the mixing mode problems associated with EMD. However, EEMD has some weaknesses under different assumptions, such as residual noise, reconstruction error and different number of modes at different realisations [44]. Another noise-assisted version of the signal decomposition technique, called complete EEMD, was proposed by Torres et al. [45] to deal with the reconstruction error from the EEMD and to enhance its performance and efficiency by undertaking exact attenuation of the residual noise in the reconstruction process. In this technique, pairs of white noise (positive and negative) are added to the original signal to produce two sets of ensemble IMFs. The procedure for extracting two sets of mixtures, M_1 and M_2, using complete ensemble EMD can be derived by

$$\begin{bmatrix} M_1 \\ M_2 \end{bmatrix} = \begin{bmatrix} 1 & 1 \\ 1 & -1 \end{bmatrix} \begin{bmatrix} x(t) \\ \omega(t) \end{bmatrix} \tag{2}$$

where $x(t)$ is the time-series signal, $\omega(t)$ is the additive while noise, M_1 is the sum of the time-series signal with positive noise and M_2 is the sum of the time-series signal and the negative noise. It is clear from Eq. (2) that the final IMF is the ensemble of both M_1 and M_2 with positive and negative residues of added white noises, thereby reducing residual noise in the reconstructed signal. Figure 3 demonstrates generating seven IMFs of the signal of interest using complete EEMD technique with 100 realisations and 100 iterations.

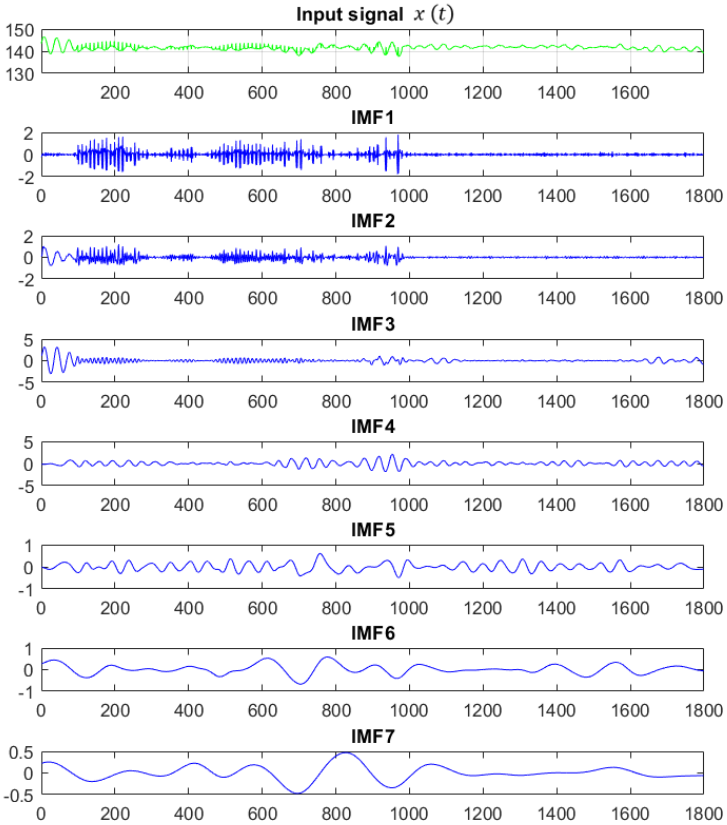

Figure 3. Signal decomposition based on the complete EEMD technique

2.3.4. Independent component analysis (ICA)

ICA is a statistical signal processing technique for solving the blind source separation (BSS) problems and is widely used to remove noise artefacts from biomedical signals [46-48]. ICA-based BSS is used

to separate the mixed source signals and retrieve the original sources using high-order statistics. Figure 4 presents the basic scheme diagram of the ICA-based BSS.

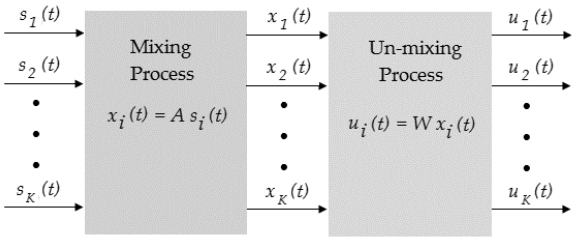

Figure 4. Basic scheme diagram of the ICA-based BSS technique

To understand how ICA operates as the BSS, assume there are K sources independently transmitting signals, $s_i(t) = [s_1(t), s_2(t), \ldots, s_K(t)]$. The observed signals, $x_i(t) = [x_1(t), x_2(t), \ldots\ldots, x_K(t)]$, by different sensors, $i = 1,2 \ldots, K$, can be expressed as follows [49]:

$$x_i(t) = As_i(t) = \sum_{i=1}^{K} (a_i s_i(t) + n_i(t)) \tag{3}$$

where A is the unknown mixing matrix with column vectors a_i, and $n_i(t)$ is the additive noise. The observations, $x_i(t)$, are now linear combinations or mixtures of the sources, $s_i(t)$. The ICA can solve the BSS problem under an assumption that all sources are statistically independent of each other. To recover the source signals, $u_i(t)$, the following expression can be used:

$$u_i(t) = Wx_i(t) = W[As_i(t)] \approx s_i(t) \tag{4}$$

where W is the un-mixing weight matrix with column vectors, w_i.

The IMF components with the best cardiopulmonary frequency bands (IMF4, IMF5 and IMF6) were chosen as inputs to ICA technique as demonstrated in Figure 5.

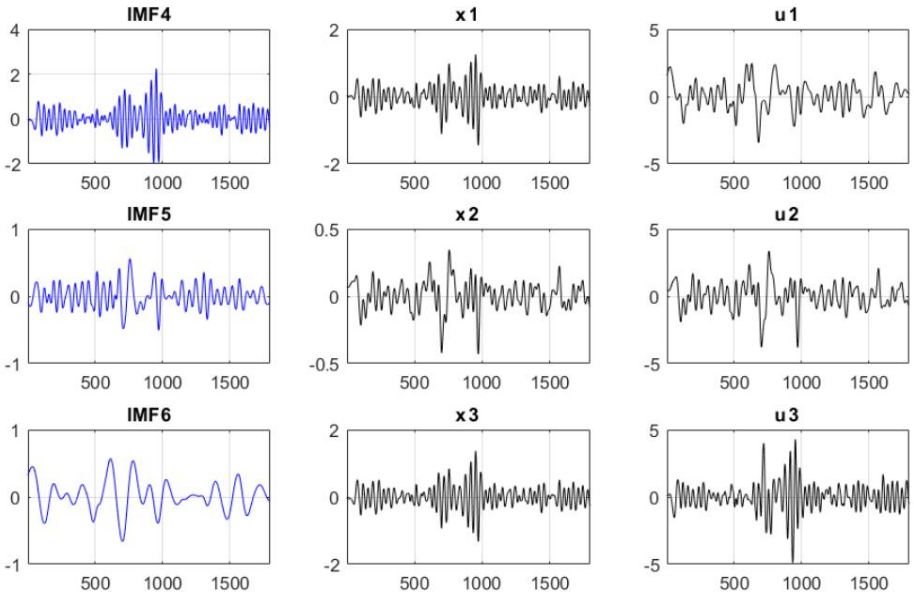

Figure 5. The signals based on ICA technique

The fast Fourier transform (FFT) was used as frequency spectrum analysis to inform the estimation of the cardiopulmonary signal by selecting the best component of the ICA outputs (u3), which has the most resemblance to the expected cardiopulmonary signal. This process was followed by two band-pass filters with selected frequencies of 0.5 to 3 Hz (30-180 beats/min) and 0.15 to 0.4 Hz (9-24 breaths/min). After the filtration, the inverse FFT was applied to obtain the temporal signals of the cardiopulmonary activity. Finally, MATLAB built-in peak detection function [50] was used to determine the number of peaks of the temporal signal and calculated the heart and respiratory rates per minute.

3. Experimental results and discussion

The experimental results and statistical readings of the proposed measurement system for two scenarios (static and dynamic scenarios) were discussed in this section. The limits of agreement (95% confidence intervals), coefficients of correlation and error ratios were calculated using the Bland-Altman plot [51], Pearson's correlation coefficient (PCC), Spearman's rank correlation coefficient (SCC), Kendall rank correlation coefficient (KCC), mean absolute error and root mean square error. All statistical readings were considered when there is no random signal included. The statistics related to HR measurements for the video data captured by the UAV for the static and dynamic scenarios are shown in Figure 6.

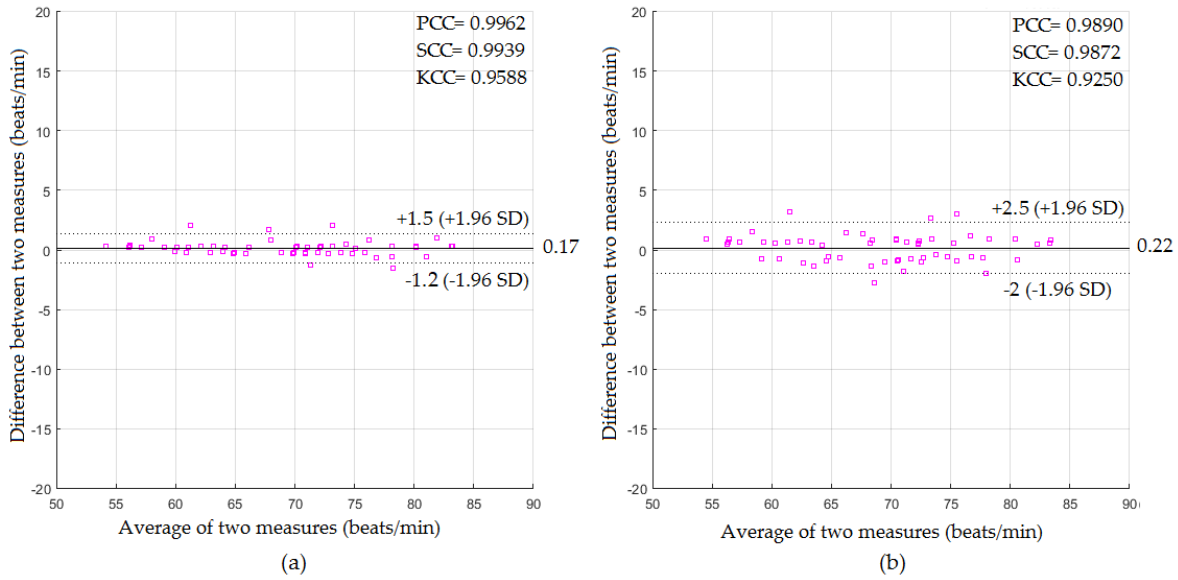

Figure 6. Bland-Altman plot of the cardiac measurements using (a) static scenario, (b) dynamic scenario

Using the data captured from the participants in the static scenario as demonstrated in Figure 6 (a), the mean difference (bias), lower and upper limits of agreement between the cardiac measurements were 0.17, −1.2 and +1.5 beats/min with correlation coefficients of 0.9962, 0.9939, 0.9588 for the PCC, SCC and KCC respectively, and error ratios of 0.52 beats/min and 0.7 beats/min for the mean absolute error and root mean square error, respectively. For the data of the dynamic scenario as demonstrated in Figure 6 (b), the mean difference, lower and upper limit of agreement were 0.22, −2 and +2.5 beats/min with PCC of 0.989, SCC of 0.9872, KCC of 0.925, the mean absolute error of 0.99 beats/min and the root mean square error of 1.16 beats/min.

The statistics related to RR measurements for the video data captured by the UAV for the static and dynamic scenarios are shown in Figure 7.

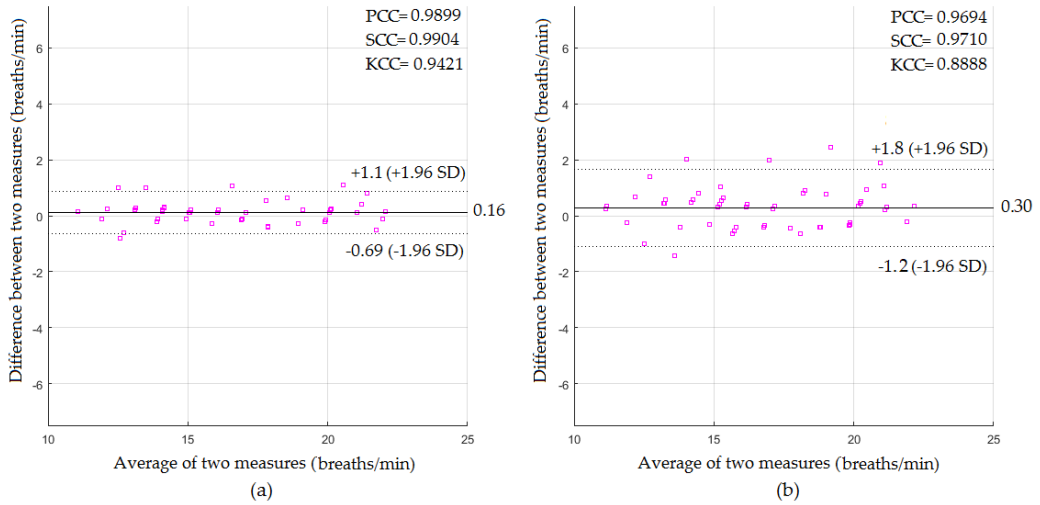

Figure 7. Bland-Altman plot of the respiratory measurements using (a) static scenario, (b) dynamic scenario

Using the data captured from the participants in the static scenario as demonstrated in Figure 7 (a), the mean difference, lower and upper limit of agreement between the respiratory measurements were 0.16, −0.69 and +1.1 breaths/min with correlation coefficients of 0.9899, 0.9904, 0.9421 for the PCC, SCC and KCC respectively, and error ratios of 0.36 breaths/min and 0.46 breaths/min for the mean absolute error and root mean square error, respectively. For the data of the dynamic scenario as demonstrated in Figure 7 (b), the mean difference, lower and upper limit of agreement were 0.3, −1.2 and +1.8 breaths/min with PCC of 0.9694, SCC of 0.971, KCC of 0.8888, the mean absolute error of 0.65 breaths/min and the root mean square error of 0.81 breaths/min.

There are many potential applications of the research presented in this study. Some of the prominent examples include using the system as a lifesaver in disaster zones or warzones, (e.g. field triage of the wounded people), assistance in security and quarantine checkpoints, and also other crowded controlled regions when people are standing or prone with only modest movement. It would also be an important addition to the future robots to be able to detect the physiological parameters of any number of people at different distances.

4. Conclusion

In this study, a computer vision-based system for extracting the human cardiopulmonary signal (HR and RR) from a hovering UAV was proposed. The proposed system used the video magnification technique to magnify the invisible skin colour variations resulting from the pressure changes during the cardiac cycle in the facial region, and applied the complete EEMD technique to decompose the signal of interest into a set of IMF components, while the most informative components were chosen as inputs to the ICA technique and removed the IMF components that fall outside of the frequency bands of interest. The experimental results demonstrated that the proposed system is a feasible solution for remote sensing assessment when the contact with the subject is difficult or impossible in certain situations.

References

[1] Zhao F, Li M, Qian Y, Tsien J Z. Remote measurements of heart and respiration rates for telemedicine. PloS One 2013; 8(10): e71384

[2] De Haan G, Van Leest A. Improved motion robustness of remote-PPG by using the blood volume pulse signature. Physiological Measurement 2014; 35(9): 1913

[3] Butler M, Crowe J, Hayes-Gill B, Rodmell P. Motion limitations of non-contact photoplethysmography due to the optical and topological properties of skin. Physiological Measurement 2016; 37(5): N27

[4] Alnaji A, Gibson K, Chahl J. Remote sensing of physiological signs using a machine vision system. Journal of Medical Engineering and Technology 2017; 41(5): 396-405
[5] Ali A, Chahl J. Contactless cardiac activity detection based on head motion magnification. International Journal of Image and Graphics 2017; 17(1): 1750001
[6] Ali A, Chahl J. Noncontact heart activity measurement system based on video imaging analysis. International Journal of Pattern Recognition and Artificial Intelligence 2017; 31(2): 1-21
[7] Scalise L, Morbiducci U. Non-contact cardiac monitoring from carotid artery using optical vibro-cardiography. Medical Engineering and Physics 2008; 30(4): 490-497
[8] Morbiducci U, Scalise L, De Melis M, Grigioni M. Optical vibrocardiography: a novel tool for the optical monitoring of cardiac activity. Annals of Biomedical Engineering 2007; 35(1): 45-58
[9] Lohman B, Boric-Lubecke O, Lubecke V, Ong P, Sondhi M. A digital signal processor for Doppler radar sensing of vital signs. Engineering in Medicine and Biology Magazine, IEEE 2002; 21(5): 161-164
[10] Kaplan A, OrSullivan J, Sirevaag E J, Lai P, Rohrbaugh J W. Hidden state models for noncontact measurements of the carotid pulse using a laser doppler vibrometer. IEEE Transactions on Biomedical Engineering 2012; 59(3): 744-753
[11] Huang M, Liu J, Xu W, Gu C, Li C, Sarrafzadeh M. A self-calibrating radar sensor system for measuring vital signs. IEEE Transactions on Biomedical Circuits and Systems 2016; 10(2): 352-363
[12] Birsan N, Munteanu D.-P. Non-contact cardiopulmonary monitoring algorithm for a 24 GHz Doppler radar. Annual International Conference of the IEEE in Engineering in Medicine and Biology Society (EMBC), 2012
[13] Abbas A, Heiman K, Orlikowsky T, Leonhardt S. Non-contact respiratory monitoring based on real-time IR-thermography. World Congress on Medical Physics and Biomedical Engineering, 2009
[14] Bennett S L, Goubran R, Knoefel F. Adaptive eulerian video magnification methods to extract heart rate from thermal video. IEEE International Symposium on Medical Measurements and Applications (MeMeA), 2016
[15] Klaessens J H, Born M, Veen A, Sikkens Kraats J, Dungen F A, Verdaasdonk R M. Development of a baby friendly non-contact method for measuring vital signs: First results of clinical measurements in an open incubator at a neonatal intensive care unit. SPIE BiOS, 2014
[16] Murthy R, Pavlidis I, Tsiamyrtzis P. Touchless monitoring of breathing function. 26th Annual International Conference of the IEEE Engineering in Medicine and Biology Society, 2004
[17] Pavlidis I, Dowdall J, Sun N, Puri C, Fei J, Garbey M. Interacting with human physiology. Computer Vision and Image Understanding 2007; 108(1): 150-170
[18] Sun N, Garbey M, Merla A, Pavlidis I. Imaging the cardiovascular pulse. IEEE Computer Society Conference in Computer Vision and Pattern Recognition, 2005
[19] Alnaji A, Perera A G, Chahl J. Remote monitoring of cardiorespiratory signals from a hovering unmanned aerial vehicle. BioMedical Engineering OnLine 2017; 16(1): 101
[20] Chen D, Wang J, Lin K, Chang H, Wu H, Chen Y, Lee S. Image sensor-based heart rate evaluation from face reflectance using Hilbert–Huang Transform. IEEE Sensors Journal 2015; 15(1): 618-627
[21] Hsu Y, Lin Y, Hsu W. Learning-based heart rate detection from remote photoplethysmography features. IEEE International Conference on Acoustics, Speech and Signal Processing, 2014
[22] Poh M, McDuff D, Picard R W. Non-contact, automated cardiac pulse measurements using video imaging and blind source separation. Optical Society of America 2010; 18(10): 10762-10774
[23] Poh M, McDuff D, Picard R W. Advancements in noncontact, multiparameter physiological measurements using a webcam. IEEE Transactions on Biomedical Engineering 2011; 58(1): 7-11
[24] Qi H, Guo Z, Chen X, Shen Z, Wang Z. Video-based human heart rate measurement using joint

blind source separation. Biomedical Signal Processing and Control 2017; 31: 309-320
[25] Alnaji A, Gibson K, Lee S, Chahl J. Monitoring of cardiorespiratory signal: Principles of remote measurements and review of methods. IEEE Access 2017; 5: 15776-15790
[26] Alnaji A, Chahl J. Detection of cardiopulmonary activity and related abnormal events using Microsoft Kinect sensor. Sensors 2018; 18(3): 920
[27] Kranjec J, Beguš S, Geršak G, Drnovšek J. Non-contact heart rate and heart rate variability measurements: A review. Biomedical Signal Processing and Control 2014; 13: 102-112
[28] Alnaji A, Chahl J. Remote optical cardiopulmonary signal extraction with noise artifact removal, multiple subject detection and long-distance. IEEE Access 2018; 6: 11573 - 11595
[29] Lewandowska M, Rumiński J, Kocejko T, Nowak J. Measuring pulse rate with a webcam—a non-contact method for evaluating cardiac activity. Federated Conference on Computer Science and Information Systems (FedCSIS), 2011
[30] Alnaji A, Chahl J. Simultaneous tracking of cardiorespiratory signals for multiple persons using a machine vision system with noise artifact removal. IEEE Journal of Translational Engineering in Health and Medicine 2017; 5: 1-10
[31] Lin K, Chen D, Tsai W. Face-based heart rate signal decomposition and evaluation using multiple linear regression. IEEE Sensors Journal 2016; 16(5): 1351-1360
[32] Cheng J, Chen X, Xu L, Wang Z J. Illumination variation-resistant video-based heart rate measurement using joint blind source separation and ensemble empirical mode decomposition. IEEE Journal of Biomedical and Health Informatics 2017; 21(5): 1422-1433
[33] De Haan G, Jeanne V. Robust pulse rate from chrominance-based rPPG. IEEE Transactions on Biomedical Engineering 2013; 60(10): 2878-2886
[34] Wang W, Stuijk S, De Haan G. A novel algorithm for remote photoplethysmography: spatial subspace rotation. IEEE Transactions on Biomedical Engineering 2016; 63(9): 1974-1984
[35] Xu L, Cheng J, Chen X. Illumination variation interference suppression in remote PPG using PLS and MEMD. Electronics Letters 2017; 53(4): 216-218
[36] Wu H, Rubinstein M, Shih E, Guttag J, Durand F, Freeman W. Eulerian video magnification for revealing subtle changes in the world. ACM Trans. Graph. 2012; 31(4): 65
[37] Verkruysse W, Svaasand L O, Nelson J S. Remote plethysmographic imaging using ambient light. Optics Express 2008; 16(26): 21434-21445
[38] Liao S, Jain A K, Li S Z. A fast and accurate unconstrained face detector. IEEE Transactions on Pattern Analysis and Machine Intelligence 2016; 38(2): 211-223
[39] Huang N E, Shen Z, Long S R, Wu M C, Shih H H, Zheng Q, Yen N, Tung C C, Liu H H. The empirical mode decomposition and the Hilbert spectrum for nonlinear and non-stationary time series analysis. Proceedings of the Royal Society of London A: Mathematical, Physical and Engineering Sciences, 1998
[40] Blanco-Velasco M, Weng B, Barner K E. ECG signal denoising and baseline wander correction based on the empirical mode decomposition. Computers in Biology and Medicine 2008; 38(1): 1-13
[41] Chen X, Liu A, Chiang J, Wang Z J, McKeown M J, Ward R K. Removing muscle artifacts from EEG data: Multi-channel or single-channel techniques? IEEE Sensors Journal 2016; 16(7): 1986-1997
[42] Zhang X, Zhou P. Filtering of surface EMG using ensemble empirical mode decomposition. Medical Engineering and Physics 2013; 35(4): 537-542
[43] Wu Z, Huang N E. Ensemble empirical mode decomposition: a noise-assisted data analysis method. Advances in Adaptive Data Analysis 2009; 1(1): 1-41
[44] Colominas M, Schlotthauer G, Torres M E. Improved complete ensemble EMD: A suitable tool for biomedical signal processing. Biomedical Signal Processing and Control 2014; 14: 19-29
[45] Torres M E, Colominas M A, Schlotthauer G, Flandrin P. A complete ensemble empirical mode decomposition with adaptive noise. IEEE International Conference on Acoustics, Speech and Signal Processing (ICASSP), 2011

[46] Safieddine D, Kachenoura A, Albera L, Birot G, Karfoul A, Pasnicu A, Biraben A, Wendling F, Senhadji L, Merlet I. Removal of muscle artifact from EEG data: comparison between stochastic (ICA and CCA) and deterministic (EMD and wavelet-based) approaches. EURASIP Journal on Advances in Signal Processing 2012; 2012(1): 127
[47] Srivastava G, Crottaz-Herbette S, Lau K, Glover G, Menon V. ICA-based procedures for removing ballistocardiogram artifacts from EEG data acquired in the MRI scanner. Neuroimage 2005; 24(1): 50-60
[48] Zhou W, Gotman J. Removal of EMG and ECG artifacts from EEG based on wavelet transform and ICA. 26th Annual International Conference of the IEEE Engineering in Medicine and Biology Society, 2004
[49] Oja E. Applications of independent component analysis. Neural Information Processing, 2004
[50] Billauer E. Peak detection using MATLAB. Dostopno na: http://billauer.co.il/peakdet.html, 2011
[51] Bland J M, Altman D G. Statistical methods for assessing agreement between two methods of clinical measurement. International Journal of Nursing Studies 2010; 47(8): 931-936